Biosensors and Bioelectronics 46 (2013) 8–14

Contents lists available at SciVerse ScienceDirect

Biosensors and Bioelectronics

journal homepage: www.elsevier.com/locate/bios

Impedance spectroscopy—An outstanding method for label-free and real-time discrimination between brain and tumor tissue *in vivo*

Heinz-Georg Jahnke [a,*,1], Axel Heimann [1,c], Ronny Azendorf [a], Konstantinos Mpoukouvalas [b], Oliver Kempski [c], Andrea A. Robitzki [a], Patra Charalampaki [c,d]

[a] Center for Biotechnology and Biomedicine (BBZ), Deutscher Platz 5, Leipzig, Germany
[b] Institut für Mikrotechnik Mainz (IMM) GmbH, Mainz, Germany
[c] Institute of Neurosurgical Pathophysiology, Medical University Mainz, Mainz, Germany
[d] Neurosurgery Department, Medical University Graz, Graz, Austria

ARTICLE INFO

Article history:
Received 7 December 2012
Received in revised form
5 February 2013
Accepted 6 February 2013
Available online 16 February 2013

Keywords:
Impedance spectroscopy
Microelectrode array
Label-free detection
Glioblastoma multiforme
In vivo tumor detection

ABSTRACT

Until today, brain tumors especially glioblastoma are difficult to treat and therefore, results in a poor survival rate of 0–14% over five years. To overcome this problem, the development of novel therapeutics as well as optimization of neurosurgical procedures to remove the tumor tissue are subject of intensive research. The main problem of the tumor excision, as the primary clinical intervention is the diffuse infiltration of the tumor cells in unaltered brain tissue that complicates the complete removal of residual tumor cells. In this context, we are developing novel approaches for the label-free discrimination between tumor tissue and unaltered brain tissue in real-time during the surgical process. Using our impedance spectroscopy-based measurement system in combination with flexible microelectrode arrays we could successfully demonstrate the discrimination between a C6-glioma and unaltered brain tissue in an *in vivo* rat model. The analysis of the impedance spectra revealed specific impedance spectrum shape characteristics of physiologic neuronal tissue in the frequency range of 10–500 kHz that were significantly different from the tumor tissue. Moreover, we used an adapted equivalent circuit model to get a deeper understanding for the nature of the observed effects. The impedimetric label-free and real-time discrimination of tumor from unaltered brain tissue offers the possibility for the implementation in surgical instruments to support surgeons to decide, which tissue areas should be removed and which should be remained.

1. Introduction

Intracranial neoplasms include a variety of different histopathologic entities, ranging from rather benign tumors, such as meningiomas, to some of the most aggressive types of human cancer. Glioblastoma multiforme, for example, is the most frequent primary malignant brain tumor in adults and median survival is on average less than one year from the time of diagnosis (Buckner, 2003). Studies have shown that an early and precise diagnosis (Hammoud et al., 1996) is crucial for improving survival rates and quality of life in patients with brain cancer (Suh, 2010). Moreover, the removal *in toto* of $>99\%$ of the tumor volume is of great importance while at the same time minimizing trauma to healthy brain tissue (Asthagiri et al., 2007; Lacroix et al., 2001) plays a crucial role, since increased radical surgery naturally bears a higher risk of damage to important intact cerebral regions and pathways. Although neurosurgeons have been equipped with new technologic features, such as neuronavigation (Hofmann et al., 2006), and fluorescence-guided surgery (Stummer et al., 1998) the distinction between healthy and tumor cells remains challenging.

The electrical properties of biological tissues have been of great interest over the last decades (Foster and Schwan, 1989; Laufer et al., 2012) with a strong focus on the discrimination of tumor tissue and unaltered tissue (da Silva et al., 2000; Hope and Iles, 2004; Keshtkar et al., 2012). Especially for breast and prostate tumor entities several studies were performed but with limited success (Chauveau et al., 1999; Zheng et al., 2008). In contrast, the use of microelectrode arrays on single cells or cell monolayers allowed the sensitive detection of cytotoxic/degenerative effects (Jahnke et al., 2009; Krinke et al., 2009), the quantitative monitoring of signal cascade activation (Wolf et al., 2008), cell contractility (Haas et al., 2010) and ion channel activation (Panke et al., 2011).

* Corresponding author. Tel.: +49 341 9731246; fax: +49 341 9731249.
E-mail address: heinz-georg.jahnke@bbz.uni-leipzig.de (H.-G. Jahnke).
[1] These authors contributed equally to this work.

0956-5663/$ - see front matter © 2013 Elsevier B.V. All rights reserved.
http://dx.doi.org/10.1016/j.bios.2013.02.013

More recently, microelectrode-based arrays were used in impedimetric studies on 3D-cultures (Jahnke et al., 2012; Kloss et al., 2008b) and organotypic brain slice cultures (Jahnke et al., 2012) for the quantitative detection of subcellular (Seidel et al., 2012) as well as tissue structure alterations (Kloss et al., 2008a) and therefore, demonstrated the outstanding potential of this label-free and non-invasive monitoring technique. In the next step, the established microelectrode array based measurement system as well as the knowledge on cell/tissue derived impedimetric data processing and interpretation should be used for label-free *in vivo* measurements. In detail, real-time measurements were performed on a well-established *in vivo* glioblastoma rat model that is widely used (Jacobs et al., 2011), in order to detect and discriminate between C6 glioma cell line allograft inoculated rat brains and healthy tissue.

2. Materials and methods

2.1. Cell culture of the C6 glioma line

C6 glioma cells (primary rat glioma) were obtained from the Institute of Neurosurgical Pathophysiology (INcP), Mainz, Germany and cultivated in Dulbecco's modified Eagle medium (DMEM) supplemented with 1% penicillin, 1% streptomycin, 10% fetal calf serum at 37 °C and 5% CO_2 atmosphere (Life Technologies GmbH, Germany). Cells were harvested routinely after 5–10 days using Trypsin–EDTA (0.05%, 0.02%, respectively) and suspended in saline.

2.2. Animals and xenograft tumors

Prior to injection, viability of the used C6 tumor cells were assessed by trypan blue staining. For animal studies, C6 glioma 10^6 cells were implanted stereo tactically into the left frontal region of the brain of anesthetized young adult male Wistar rats (Charles River Wiga, Sulzfeld, Germany). Briefly, burr-hole trephination was carried out and a custom-designed needle was inserted for slow injection of the tumor cell suspension. Tumors were allowed to establish for 10 days on average and animals were then used for *in vivo* measurements. After this time period, animals implanted with C6 glioma cells began showing signs of apathy and fatigue. Animals were bred and kept at an animal facility in a temperature-controlled environment on a 12-h light/dark cycle and were fed a regular pelleted rodent maintenance diet and water *ad libitum*. All animal experiments were performed at the Institute for Neurosurgical Pathophysiology (Medical Center, Johannes-Gutenberg-University Mainz) in accordance with national and international guidelines and were approved by the Governmental Animal Care and Use Committee (Landesuntersuchungsamt Koblenz 23-177-07/G 10-1-050).

2.3. Surgery

An intraperitoneal catheter was placed for deep anesthesia with chloral hydrate. Craniotomy was performed after fixing the animals in a stereotactic frame and an intracranial window was placed to expose the tumor, the transition zone and healthy brain tissue, while bleeding was controlled using heat-coagulation, TABOTAMP® and bone wax (Henry Schein VET, Hamburg, Deutschland). After *in vivo* measurements, the rats were sacrificed and the brain was removed for further histopathology.

2.4. Microelectrode array-based impedance spectroscopy

For exploring the feasibility of impedimetric detection and discrimination of brain and tumor tissue, we used our self-developed impedance measurement system. Based on the high precision impedance analyzer Agilent 4294A (Agilent Technologies) and our self-developed 32 channel multiplexer system we used a polyimide substrate-based flexible microelectrode-array (MultichannelSystems, Reutlingen, Germany) with a thickness of 30 μm and a width of 2 mm. The electrode array on the top of the *in vivo* sensor, consists of 32 titanium nitride measurement electrodes (30 μm diameter, 300 μm interspacing) with a nanocolumnar surface structure and two counter electrodes. To obtain an optimum contact of the tissue, the flexible sensor was fixed to a glass rod, while the electrode array itself was bendable around the rounded tip of the glass rod and was fixed to a micrometer stage. So, the sensor could precisely be approached to the target tissue and contact it with a defined pressure, being kept constant for the performed measurements. To prevent blood clotting on the microelectrode array that leads to a nearly complete loss of tissue signal, the microelectrode array and the tissue was extensively rinsed with 0.9% NaCl solution (Life Technologies GmbH, Germany). From the sensor array, impedance spectra were recorded from 28 electrically contacted electrodes via the multiplexer and the impedance analyzer, synchronized by an Atmega32-based microcontroller. Impedance spectra *i.e.* impedance magnitude and phase angle for each electrode were recorded in the frequency range from 500 Hz to 5 MHz (51 points) with an amplitude of 10 mV using our self-developed recording software IMAT v1.8g (Impedance Measurement and Automation Tool). The recorded data was analyzed by our self-developed software IDAT v.3.6 (Impedance Data Analyzing Tool). The system impedance (without tissue) was obtained by measurement with microelectrode array dipped into phosphate buffered saline PBS). The tissue contribution to the impedance magnitude was extracted by automated calculation of the relative impedance $(|Z|_{\text{with tissue}} - |Z|_{\text{without tissue}})/\ |Z|_{\text{without tissue}}\ x\ 100\%)$ and the maximum relative impedance (peak) was determined by the IDAT v3.6 software. From the 28 recorded electrodes, electrodes that showed a maximum in the range of the base line level (depending on the measurement—in the range of 20–50% maximum relative impedance) were automatically removed (no sufficient contact to the tissue). If there were less than 15 electrodes the measurement was not used for the statistical analysis. The validated electrodes of one contacting were averaged. For obtaining a robust characteristic spectrum each tissue sample was contacted four times. The averaged spectrum of each contacting was averaged for statistical analysis.

2.5. Statistics

All statistical analyses were done using Graphpad Prism 5. In general, all values are given as means (±) s.e.m (standard error of the mean) unless described differentially. Multiple group comparisons were analyzed by two-way ANOVA and Bonferroni *post hoc* test. Comparisons between two groups were analyzed by the Mann–Whitney test. Differences between two means with $p < 0.05$ were considered as significant, $p < 0.01$ very significant and $p < 0.001$ extremely significant.

3. Results and discussion

3.1. Design of the in vivo measurement system

Before starting the *in vivo* measurements we had to establish an appropriate measurement setup. First we investigated in a microelectrode array that could be used on undefined shaped tissue structures while ensuring sufficient electrode/tissue contact for a reliable measurement signal. In this context, we identified a flexible

microelectrode array based on a polyimide substrate with 28 measurement electrodes (30 μm in diameter). The electrodes were made of nanocolumnar structured titanium nitride resulting in reduced impedance. While these microelectrode arrays were developed for the electrophysiological recording we found out that it is perfectly suitable for highly sensitive impedance spectroscopy on tissue samples. In our established setup we used a computer controlled single channel high precision impedance analyzer in combination with our self-developed 32-channel multiplexer (Fig. 1A). To further lowering the impedance of the measurement setup and to achieve an optimum tissue penetration of the electrical field and coverage, both ground electrodes on the microelectrode array were connected in parallel to the counter electrode input of the multiplexer. The flexible microelectrode array was fixed on a glass rod while the microelectrode array at the top of the substrate was flexible bend over the rod tip. This allows a feasible contacting of the tissue by approximation of the glass rod to the brain using a micrometer stage (Fig. 1B).

3.2. Impedimetric discrimination between unaltered brain tissue and tumor tissue

Since the tumor cells were stereotactically injected into the left hemisphere, tumor and unaltered brain tissue could be directly measured in serial contactings on each animal (Fig. 2A). To get a better impression on the tumor tissue integration and composition single brains were fixed, cryodissected and immunocytochemical stained after the experiment (Fig. 2B). By using the neuron-specific axon marker neurofilament 200 the image revealed a clearly distinguishable and well integrated tumor on the left hemisphere. To determine the impedance of the measurement system itself the electrode array was dipped into phosphate buffered saline (afterwards noticed as "system"). For a reliable characterization and discrimination of unaltered brain and tumor tissue all electrodes ($n \geq 15$) from one measurement were averaged resulting in a mean value for a tissue area of 2 mm × 2 mm and a penetration depth of the electrical field of approximately 1 mm. For each condition (unaltered brain, tumor) the sensor was contacted and removed four times to and from the target tissue. Furthermore, the mean spectra of these four contactings were averaged. The impedance magnitude as well as the phase angle spectra of the tissue showed clearly different characteristics than the spectra obtained from the system (Fig. 2B).

Although there were small differences between tumor and unaltered brain tissue derived impedance spectra observable, the extraction of the tissue contribution (relative impedance) from the impedance magnitude spectra revealed additional tissue specific differences (Fig. 2C). The unaltered brain tissue showed a characteristic relative impedance spectrum with a maximum of 170.9 ± 8.2% at 18.8 ± 0.5 kHz that were higher than the maximum of the tumor tissue with 129.1 ± 10.5% at 20.1 ± 0.7 kHz. More strikingly, the unaltered brain tissue revealed a characteristic plateau in the frequency range of 100–500 kHz that could never be observed in the spectra of tumor tissue. To include this neuronal tissue specific plateau into the numeric comparison the relative impedance at 315 kHz were used (unaltered brain tissue 87.5 ± 3.2% *vs.* tumor tissue 49.3 ± 2.2%). With regard to the observed differences we studied the reliability and the dependency of the observed effects (especially for the relative impedance maximum) from the contacting conditions (Fig. S1). Therefore, we contacted unaltered brain tissue by approximation of the flexible microelectrode-array (Fig. S1B) using a micrometer stage as done for all experiments. After recording of the impedance spectra we retracted the glass rod in 0.5 mm steps and measured again. The calculated relative impedance spectra revealed a reproducible signal until a retraction of the glass rod of 1.5 mm from the tissue (Fig. S1A). Interestingly, the maximum relative impedance did not decreased; instead a small increase was observed (all values are listed in Table. S1). This behavior could be explained by the flexible bending of the microelectrode array over the rod tip. When the glass rod was in direct contact with the tissue the flexible array is pressed against the tissue with a certain degree of fitting to the surface structure of the contacted tissue. When the glass rod was retracted the tension within the polyimide foil of the bended microelectrode array was sufficient enough for achieving an optimum tissue contacting (Fig. S1C). In comparison to the direct pressing on the tissue surface by the glass rod an even better fitting of the polyimide substrate to the tissue could be achieved. Moreover, a further retraction of 0.5 mm (to 2.5 mm) leads to an immediate decrease of the relative impedance to the base line of 20–50% (depending on the electrode) that reflects the contribution of the rinse buffer and residual blood on the tissue. There was no distance dependent moderate impedance decrease observable. Taken together, this contacting dependent tissue signal behavior shows a superior and certain contacting distance independent stability while a loss of the contact could be easily detected by an immediate decrease of the relative impedance to the base line.

3.3. Statistical analysis of characteristic impedance spectrum parameters

For verification of the observed characteristic differences between unaltered brain tissue and tumor tissue we repeated the measurement on three further rats and processed the data in

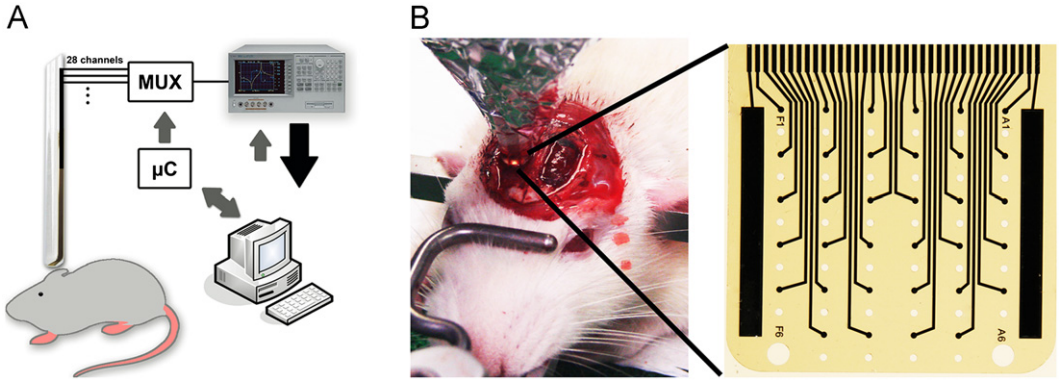

Fig. 1. Microelectrode array-based measurement system for *in vivo* tumor tissue detection. (A) Scheme of the measurement setup: 28 electrodes of the sensor were connected to our self-developed multiplexer (MUX) which was connected to the high precision impedance analyzer. Synchronized switching of the electrodes and the impedance analyzer was realized by a microcontroller. (B) The sensor was fixed to a rounded glass rod with the electrode array bendable around the glass rod tip. For the measurement the cranium was opened and the flexible microelectrode array was brought in direct contact with the brain or tumor tissue. The microelectrode array is based on a flexible polyimide substrate with a width of 2 mm and the electrode array is based on 32 titanium nitride electrodes with (30 μm diameter) with an interspacing of 300 μm.

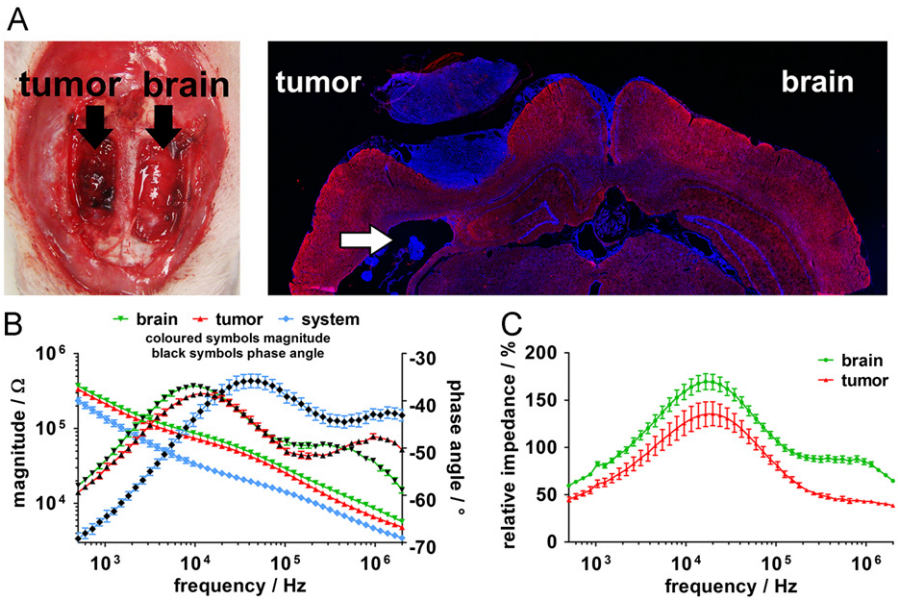

Fig. 2. Impedimetric characteristics of the measurement setup, unaltered brain and tumor tissue. (A) Opening of the cranium revealed the tumor on the left hemisphere and unaltered brain tissue on the right hemisphere. For detailed information on tumor spreading, the brain was cryodissected and stained (right) for neurofilament-200 (red) and cell nuclei (blue). The arrow indicates migrated tumor cells into the left ventricle. (B) For the bioelectronic identification of tumor tissue impedance magnitude and phase angle spectra of the system, unaltered brain and tumor were recorded (mean ± s.e.m., $n=4$ contactings on one rat). (C) The elimination of the system contribution by calculation of the relative impedance revealed distinct differences within the characteristic spectrum shape for the unaltered brain and tumor tissue ($n=4$ contactings on one rat). (For interpretation of the references to color in this figure legend, the reader is referred to the web version of this article.)

the same way like for the first rat (Fig. S2). The statistical analysis for each rat with $n=4$ contactings per tissue type revealed a reduced (Fig. 3A) and shifted relative impedance maximum. For the relative impedance maximum values the differences were significant for all rats with exception of rat 3. Furthermore, for all rats a clearly visible higher plateau was observable in the unaltered brain tissue at higher frequencies (100–500 kHz) (Fig. S2). The comparison of unaltered brain tissue and tumor tissue revealed for all rats significant higher relative impedance values at 315 kHz (all values are listed in Table S2). For a comprehensive statistical analysis the tumor tissue values were normalized to the appropriate unaltered brain tissue values (100%) for each rat (Fig. 3B). The analysis of significance revealed a significant decreased relative impedance maximum (73.5 ± 5.4%) as well as significant reduced relative impedance at 315 kHz (56.9 ± 1.3%). For the tumor tissue the frequency shift of the maximum relative impedance was significant with 112.2 ± 3.3%. While the statistical analysis of unaltered brain tissue and tumor tissue over all revealed significant differences for each of the three parameters in an individual case one parameter alone (*e.g.* maximum relative impedance—rat 3) could be not enough for discrimination. But taken all three parameters into account the discrimination in each case was possible. With regard to patient specific identification of tumor tissue real-time multivariate analysis of the identified parameters could provide reliable information during a surgery for the decision to remove the tissue or not.

3.4. *Equivalent circuit model for explanation of tissue specific characteristics*

In order to get a more detailed insight into the nature of the observed specific impedance spectra characteristics we wanted to apply an equivalent circuit model. Since the investigated biological system was extremely complex in its structure *i.e.* due to the presence of tissue, blood cells, tumor cells, intracellular and extracellular components, cell membranes as well as phosphate buffered saline and the complex electrical properties of the flexible microelectrode array itself, a simplification of the equivalent circuit model was necessary. The microelectrode cell interface for 2D cultures can be well described by a simple equivalent circuit (Jahnke et al., 2009; Krinke et al., 2009) consisting of an constant phase element (CPE) and a serial resistance for the measurement system and the electrode–electrolyte interface. The cell membrane could be described by a capacitance and resistance in parallel and the culture medium by a resistance. But in this study, this extremely simplified equivalent circuit model did not allow a sufficient fitting of the measured spectra and moreover, could not reflect the characteristic spectra shape of the unaltered brain tissue. We had to introduce a further capacity that reflects the stray effects of the circuit pathways as well as the inactive electrodes within the microelectrode array (Thielecke et al., 2001) that spreads over the monitored tissue (Fig. S3A). Furthermore, we had to include a further resistance in series (R_{Extra}) that reflects the summed up extracellular resistance between the parallel cellular capacitance and resistance units. Without this tissue dependent parameter the unaltered brain tissue specific spectra characteristics could not be retrieved. In combination with a CPE and resistance for the electrode–electrolyte system, we achieved an excellent fitting of the impedance magnitude spectra as well as a good fitting of the impedance phase angle spectra in the frequency range of 1–500 kHz (Fig. 4A). More strikingly, using this equivalent circuit model for parameter fitting and thereof, the calculated magnitude spectra for system, brain and tumor tissue we obtained the characteristic relative impedance spectra for the tumor tissue and especially, for the unaltered brain tissue (Fig. S3B). These spectra were comparable to the spectra retrieved from the measured data (Fig. 2C).

For the equivalent circuit parameter analysis we used the measured data of rat #1. The magnitude and phase angle spectra of each contacting were fitted using a self-written software (LabView, National Instruments). The program obtained the parameters by minimizing the sum of residuals using an unconstrained optimization function (Downhill–Simplex algorithm). For the final equivalent circuit model (Fig. S3A) the complex impedance Z used in the fitting procedure is given by

$$Z = \{i\omega C_{Stray} + [R_{Buf} + Z_{CPE\ El} + (1/R_{Tissue} + i\omega C_{Tissue})^{-1}]^{-1}\}^{-1} + R_{Extra} \quad (1)$$

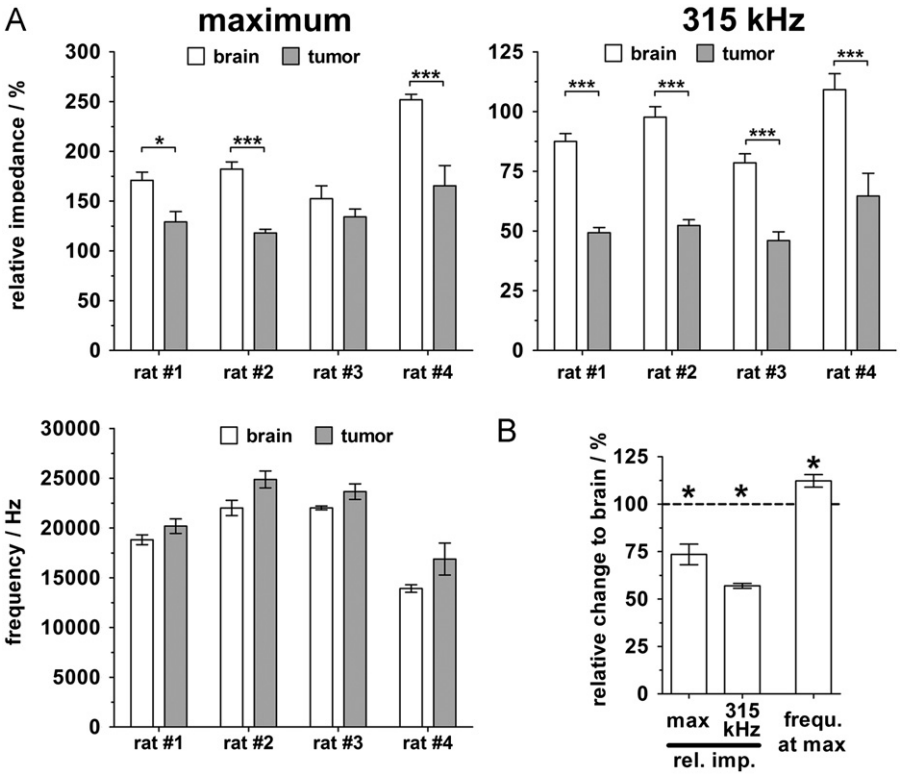

Fig. 3. Impedance spectra analysis of four rats reveals characteristic differences between unaltered brain tissue and tumor tissue. (A) The statistical analysis on each individual rat revealed significant effects for the relative impedance maximum and the relative impedance at 315 kHz while the frequency at which the maximum relative impedance occurred does not (n=4 contactings per rat). (B) For statistical comparison of all rats the values of the tumor tissue were normalized to the appropriate unaltered brain tissue values (100%) (n=4 rats).

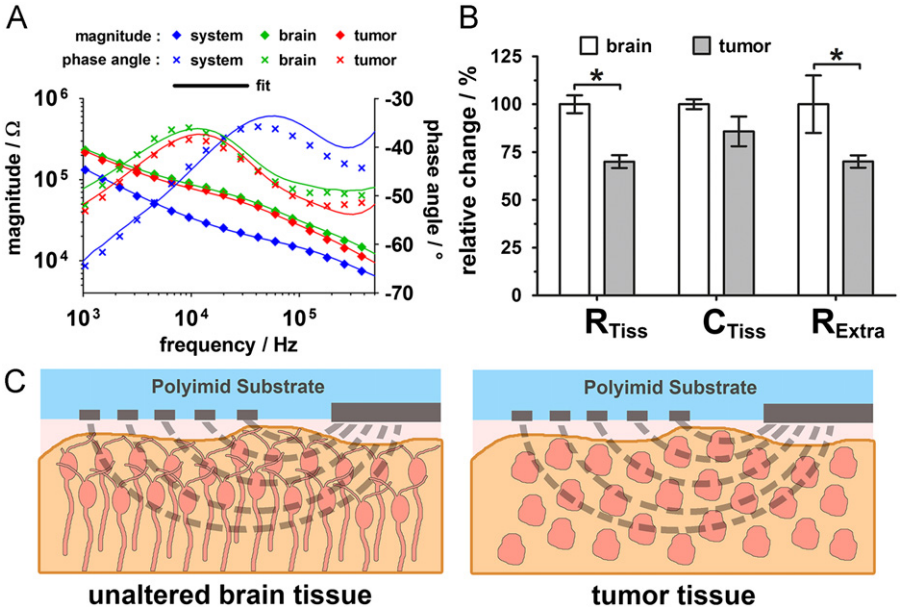

Fig. 4. Equivalent circuit model for the description of the tissue specific impedimetric properties. (A) The specific equivalent circuit parameters for the system, the unaltered brain tissue and the tumor tissue were obtained by numeric optimization using the measured impedance magnitude and phase angle data. (B) The calculated parameters of all four contactings on one rat were determined and normalized to the unaltered brain tissue values (mean ± s.e.m.). (C) The specific impedimetric characteristics of unaltered brain tissue could be explained with the unique brain tissue composition that comprises dense neuron networks with a high content of axonal and distal processes while the tumor tissue consists of cells with a smaller membrane surface to volume ratio and edema.

Within this equation $Z_{\mathrm{CPE\ El}}$ is described as $A^{-1}(i\omega)^{-n}$ with the fitting parameters A and n and $\omega=2\pi f$ as the angular frequency and i as the imaginary unit (Jahnke et al., 2009). For the system the same equivalent circuit was used without the tissue dependent parameters C_{Tissue}, R_{Tissue} and R_{Extra}. Therefore, mean values of 10 nSs^{-n} for A and 0.7 for n were obtained. These values are in line with previously determined values for nanocolumnar structured electrode surfaces (Krinke et al., 2009) that are reflected by values for $n<1$. The fitting of the unaltered brain tissue and tumor tissue derived impedance spectra revealed for the averaged

(n=4) CPE_{El} parameter A values of 13 nSs^{-n} (brain) as well as 11 nSs^{-n} (tumor) and for n values of 0.68 (brain) as well as 0.71 (tumor). For the parameter R_{Buf} we obtained mean values of 26 kΩ (brain) and 23 kΩ (tumor) and for C_{Stray} values of 29 pF (brain) as well as 32 pF (tumor). Furthermore, for the tissue specific parameters we obtained 125 pF (brain) and 122 pF (tumor) for C_{Tissue}, 30 kΩ (brain) and 25 kΩ (tumor) for R_{Tissue} as well as 5.2 kΩ (brain) and 3.6 kΩ (tumor) for R_{Extra}. For the statistical analysis of significant differences between the unaltered brain tissue and tumor tissue derived equivalent circuit parameter we normalized all values of both tissue types to the appropriate mean values of the unaltered brain tissue (100%) (Table S2). For the CPE_{El} parameter A we obtained an insignificantly lower value of 80.7% for tumor tissue and for n an insignificantly higher value of 104.7%. For C_{Stray} a higher value of 110.2% was obtained for tumor tissue which was statistically not significant and for R_{Buf} a decreased value of 91.2% which was not significant likewise. For the tissue specific parameters (Fig. 4B) we retrieved a significantly decreased value for R_{Tissue} with 70.0% for the tumor tissue and for R_{Extra} a significantly decreased value of 70.1%. For C_{Tissue}, there was a decrease to 85.8% in the tumor tissue observable but again without significance.

Taken together, the results of the statistical analysis, revealed only significant changes for the tissue specific parameters R_{Tissue}, R_{Extra} and a tendency for the tissue specific parameter C_{Tissue}. All other parameters showed no significant differences of 10% or less with exception of the CPE parameter A (20%). This validates the chosen equivalent circuit model since so observed impedance spectra alterations should be mainly caused by tissue specific differences. Based on the observed parameter changes we developed a model for the impedance spectroscopy-based discrimination of unaltered brain and tumor tissue (Fig. 4C). While the unaltered brain tissue is mainly composed of highly organized neurons with long distal and axonal processes (see neurofilament staining Fig. 2A), the tumor tissue consists of tumor cells with a more spherical but irregular shape. Moreover, the membrane of neuronal cells offers special characteristics with regard to their electrogenic and functional properties. These differences could be an explanation for the observed reduced R_{Tissue}, C_{Tissue} values in the tumor tissue. Although the immunocytochemical staining provides no clear evidence for a reduced cell density in the tumor tissue overall, it is known that tumor cells induce reduction of adhesion molecules as well as cell–cell contacts (Teodorczyk and Martin-Villalba, 2010) and actively degenerate extracellular matrix structures by enzyme secretion (Baba and Catoi, 2007; Teodorczyk and Martin-Villalba, 2010). This leads to an increased migration and invasion into further tissues also seen on the immunocytochemical staining (Fig. 2A, arrow). This processes leads to a drastically decreased extracellular resistance and therefore, to the observed decreased R_{Extra} in tumor tissue. Moreover, in different tumor tissues brain edema is regularly present (Skourou et al., 2007) which could also contributes to a lowered extracellular resistance. Taken together, we have evidences that the unique structure of neuronal cells and their organization in brain tissue allows the discrimination from tumor tissue such as glioblastoma using impedance spectroscopy.

In this context, we investigated complementary to the present study, other diagnostic methods on exactly the same tumor model, aiming to differentiate between unaltered and malignant brain tissue. Even though the findings are preliminary, it was found that confocal laser endomicroscopy (Foersch et al., 2013), two photon microscopy (Riemann et al., 2013) and haptic differentiation by means of torsional resonators (Johannsmann, 2012) are very promising, and could, after sufficient development, become eligible candidates for an implementation into surgical instruments aiming to support the surgeon's decisions, whether suspicious tissue should be removed or not.

4. Conclusions

In this study we could demonstrate that impedance spectroscopy is a feasible method to identify tissue types. More strikingly, the impedance spectroscopy based label-free and real-time measurement on a glioblastoma rat model revealed unique impedance spectra characteristics for unaltered brain tissue that could be used for the discrimination from tumor tissue. In our study on several rats we could significantly distinguish for each rat functional neuronal tissue from tumor tissue by analysis of the maximum tissue contribution in the range of 10–20 kHz and moreover, the neuron tissue specific plateau in the frequency range of 100–500 kHz that is here described for the first time. In tumor tissue this plateau was diminished and a hint for the loss of functional neuronal tissue organization/composition as well as transformation. In this context, we established an equivalent circuit model for a more detailed description of tissue specific electrical parameters that are responsible for the tissue specific impedance spectra characteristics. Based on the used flexible microelectrode array system, this approach offers the opportunity to adapt the array structure for specific needs *e.g.* future endoscopic surgery instruments. So analysis area as well as penetration depth of the electric field can be modulated. Moreover, the used microelectrodes were developed for field potential measurements and therefore, a combined measurement system could be used for the impedimetric discrimination of tumor tissue and field potential monitoring to identify sections of the brain with highly active neuronal networks which should be spared from surgery.

Acknowledgements

We would like to thank Pr. G. Wegner, Dr. P. Detemple and Dr. P. Papadopoulos for their helpful discussions and B. Kempski and A. Ehlert for technical assistance. This work was funded by the German Research Foundation (DFG; SFB610, Z5 Rob.) and a governmental grant from the German Federal Ministry of Education and Research (No. 16SV5069) to O.K.

Appendix A. Supporting information

Supplementary data associated with this article can be found in the online version at http://dx.doi.org/10.1016/j.bios.2013.02.013.

References

Asthagiri, A.R., Pouratian, N., Sherman, J., Ahmed, G., Shaffrey, M.E., 2007. Neurologic Clinics 25 (4), 975–1003 viii-ix.
Baba, A.I., Catoi, C., 2007. Comparative Oncology.
Buckner, J.C., 2003. Seminars in Oncology 30 (6 Suppl 19), 10–14.
Chauveau, N., Hamzaoui, L., Rochaix, P., Rigaud, B., Voigt, J.J., Morucci, J.P., 1999. Annals of the New York Acadamy of Sciences 873, 42–50.
da Silva, J.E., de Sa, J.P., Jossinet, J., 2000. Medical and Biology Engineering and Computing 38 (1), 26–30.
Foersch, S., Heimann, A., Ayyad, A., Spoden, G.A., Florin, L., Mpoukouvalas, K., Kiesslich, R., Kempski, O., Goetz, M., Charalampaki, P., 2012. PLoS One 7 (7), e41760.
Foster, K.R., Schwan, H.P., 1989. Critical Reviews in Biomedical Engineering 17 (1), 25–104.
Haas, S., Jahnke, H.G., Glass, M., Azendorf, R., Schmidt, S., Robitzki, A.A., 2010. Lab on a Chip 10 (21), 2965–2971.
Hammoud, M.A., Sawaya, R., Shi, W., Thall, P.F., Leeds, N.E., 1996. Journal of Neuro-oncology 27 (1), 65–73.
Hofmann, U.G., Folkers, A., Mosch, F., Malina, T., Menne, K.M., Biella, G., Fagerstedt, P., De Schutter, E., Jensen, W., Yoshida, K., Hoehl, D., Thomas, U., Kindlundh, M.G., Norlin, P., de Curtis, M., 2006. IEEE Transactions on Biomedical Engineering 53 (8), 1672–1677.
Hope, T.A., Iles, S.E., 2004. Breast Cancer Research 6 (2), 69–74.
Jacobs, V.L., Valdes, P.A., Hickey, W.F., De Leo, J.A., 2011. ASN NEURO 3 (3), e00063.

Jahnke, H.G., Braesigk, A., Mack, T.G., Ponick, S., Striggow, F., Robitzki, A.A., 2012. Biosensors and Bioelectronics 32 (1), 250–258.
Jahnke, H.G., Rothermel, A., Sternberger, I., Mack, T.G., Kurz, R.G., Panke, O., Striggow, F., Robitzki, A.A., 2009. Lab on a Chip 9 (10), 1422–1428.
Diethelm Johannsmann, Arne Langhoff, Berthold Bode, Konstantinos Mpoukouvalas, Axel Heimann, Oliver Kempski, Patra Charalampaki Sensors and Actuators A: Physical Volume 190, 1 February 2013, Pages 25–31 http://dx.doi.org/10.1016/j.sna.2012.10.039,.
Keshtkar, A., Salehnia, Z., Somi, M.H., Eftekharsadat, A.T., 2012. Physics in Medicine and Biology 28 (1), 19–24.
Kloss, D., Fischer, M., Rothermel, A., Simon, J.C., Robitzki, A.A., 2008a. Lab on a Chip 8 (6), 879–884.
Kloss, D., Kurz, R., Jahnke, H.G., Fischer, M., Rothermel, A., Anderegg, U., Simon, J.C., Robitzki, A.A., 2008b. Biosensors and Bioelectronics 23 (10), 1473–1480.
Krinke, D., Jahnke, H.G., Panke, O., Robitzki, A.A., 2009. Biosensors and Bioelectronics 24 (9), 2798–2803.
Lacroix, M., Abi-Said, D., Fourney, D.R., Gokaslan, Z.L., Shi, W., DeMonte, F., Lang, F.F., McCutcheon, I.E., Hassenbusch, S.J., Holland, E., Hess, K., Michael, C., Miller, D., Sawaya, R., 2001. Journal of Neurosurgery 95 (2), 190–198.
Laufer, S., Solomon, S.B., Rubinsky, B., 2012. Physiological Measurement 33 (6), 997–1013.
Panke, O., Weigel, W., Schmidt, S., Steude, A., Robitzki, A.A., 2011. Biosensors and Bioelectronics 26 (5), 2376–2382.
Riemann, I., Le Harzic, R., Mpoukouvalas, K., Heimann, A., Kempski, O., Charalampaki, P., 2012. Lasers in Surgery and Medicine 44 (9), 719–725.
Seidel, D., Krinke, D., Jahnke, H.G., Hirche, A., Kloss, D., Mack, T.G., Striggow, F., Robitzki, A., 2012. PLoS One 7 (11), e49150.
Skourou, C., Rohr, A., Hoopes, P.J., Paulsen, K.D., 2007. Physics in Medicine and Biology 52 (2), 347–363.
Stummer, W., Stocker, S., Novotny, A., Heimann, A., Sauer, O., Kempski, O., Plesnila, N., Wietzorrek, J., Reulen, H.J., 1998. Journal of. Photochemistry and Photobiology B: Biology 45 (2-3), 160–169.
Suh, J.H., 2010. The New England Journal of Medicine 362 (12), 1119–1127.
Teodorczyk, M., Martin-Villalba, A., 2010. Journal of Cellular Physiology 222 (1), 1–10.
Thielecke, H., Mack, A., Robitzki, A., 2001. Fresenius Journal of Analytical Chemistry 369 (1), 23–29.
Wolf, P., Rothermel, A., Beck-Sickinger, A.G., Robitzki, A.A., 2008. Biosensors and Bioelectronics 24 (2), 253–259.
Zheng, B., Zuley, M.L., Sumkin, J.H., Catullo, V.J., Abrams, G.S., Rathfon, G.Y., Chough, D.M., Gruss, M.Z., Gur, D., 2008. Medical Physics 35 (7), 3041–3048.